Interoperable Encoding and 3D Printing of Anatomical Structures

Amaury Fierens
ICTEAM & EPL, UCLouvain
Louvain-la-Neuve, Belgium
amaury.fierens@uclouvain.be

Thibault Gregoir
EPL, UCLouvain
Louvain-la-Neuve, Belgium
thibault.gregoir@student.uclouvain.be

Sébastien Jodogne
ICTEAM & EPL, UCLouvain
Louvain-la-Neuve, Belgium
sebastien.jodogne@uclouvain.be

ABSTRACT

The rendering and printing of 3D models of anatomical structures offers a wide range of promising applications in multiple medical disciplines, in the training of medical students, as well as in patient education. The growing use of such 3D models in the clinical routine will soon imply great challenges in terms of data management, data archiving, and data exchange, since the commonplace file formats for 3D printing are not designed to store medical information, or to refer to other medical resources. This paper explores the use of the DICOM standard so that 3D models can be stored alongside standard medical images, inside a unified hospital information system, with full medical traceability and technical interoperability. A free and open-source software pipeline is introduced to generate 3D models either from binary bitmap volumes that were produced by artificial intelligence algorithms, or from contours that were manually delineated by physicians, then to encapsulate the generated models as DICOM instances. Our pipeline also features a lightweight Web viewer that is suitable for rendering DICOM STL instances by any Web browser. The results demonstrate the effectiveness of the proposed approach, highlighting successful 3D model generation and printing.

CCS CONCEPTS

• **Applied computing** → **Consumer health**; **Health informatics**; • **Human-centered computing** → *Visualization techniques*; *Visualization toolkits*; • **Computing methodologies** → **Image segmentation**; **Reconstruction**.

KEYWORDS

DICOM, 3D printing, 3D visualization, Organ segmentation

ACM Reference Format:
Amaury Fierens, Thibault Gregoir, and Sébastien Jodogne. 2023. Interoperable Encoding and 3D Printing of Anatomical Structures. In *Proceedings of 10th International Conference on Bioinformatics Research and Applications (ICBRA 2023).* ACM, New York, NY, USA, 7 pages. https://doi.org/XXXXXXX.XXXXXXX

ICBRA 2023, September 22–24, 2023, Barcelona, Spain

ACM ISBN 978-1-4503-XXXX-X/18/06…$15.00
https://doi.org/XXXXXXX.XXXXXXX

1 INTRODUCTION

3D printing has increasingly become an important topic in health informatics due to its ability to translate 3D data generated by medical imaging modalities, such as CT-scans, into physical objects. This technology notably enables healthcare professionals to enhance their understanding and visualization of personalized anatomical structures, with applications to surgical planning and simulation, as well as patients to better understand diagnoses, treatment plans, and potential outcomes in a more understandable and tangible way, fostering patient engagement and informed decision-making. 3D-printed anatomical models also serve as valuable educational tools for medical students and trainees. They offer a hands-on and realistic learning experience, allowing students to better understand human anatomy and various pathologies, which can lead to improved medical training and ultimately to better patient care.

The effectiveness of 3D printing in preoperative planning and surgical training has been extensively studied [12, 23]. Noteworthy applications include spine surgery [7], orthognathic surgery [17], endodontics [28], and treatment planning for spine and sacral tumors [20]. Very importantly, 3D printing enables the fabrication of customized implants and prosthetics tailored to individual patients. These patient-specific devices offer a better fit, reduced chances of rejection, and improved functionality compared to traditional, off-the-shelf solutions [24].

Patient education is another area where 3D printing demonstrates benefits in contexts such as general hospital care [9], dermatology [40], chronic diseases [4], oncology [11, 25], or surgery [16]. It has been shown that patient education not only enhances the quality of care and patient satisfaction but also improves compliance, staff satisfaction, and resources utilization [1, 5, 34]. Advancements in technology have opened possibilities to include virtual reality [32] and 3D printing [3]. Patient education through 3D printing has proven effective in various conditions, such as cardiac surgery [26, 31], degenerative lumbar disease [39], prostate cancer [33], renal tumors [6], hepatic tumors [38], and even Parkinson disease [2].

The generation of 3D models from medical images has traditionally been a tedious and time-consuming process. However, recent advancements in deep learning-based methods [38], especially in the automated segmentation of organs [8, 29], have the potential to facilitate the generation of 3D models in clinical environments. For instance, the generalist model TotalSegmentator can automatically segment up to 104 different anatomical structures on a 3D CT-scan [35]. Such automated algorithms for organ segmentation represent an extremely important evolution that will soon lead to a major increase in the use of 3D printing in hospitals.

Unfortunately, the use of 3D models generated from medical images is nowadays not well integrated inside the clinical workflow. This is notably visible in the fields of dentistry and orthodontics, where 3D models of dental implants are most often stored as standalone STL files on ad-hoc systems that are distinct from the Picture Archiving and Communication System (PACS) of the hospital. Moreover, STL files merely contain a list of 3D triangle facets that describe a 3D mesh. As a consequence, STL files convey no information about the patient, nor reference the medical images from which they were derived, which implies a lack of medical traceability.

For this reason, Release 2018a of the Digital Imaging and Communications in Medicine (DICOM) standard included Supplement 205 entitled "*DICOM Encapsulation of STL Models for 3D Manufacturing*." This supplement specifies how to embed a STL file inside a DICOM envelope, completing the raw 3D model with patient metadata and links to the referenced medical images. Moreover, the resulting DICOM instances can be ingested by any regular PACS, which consolidates the storage systems, hereby reducing costs and maintenance. Nevertheless, the DICOM STL standard is not widely adopted by hospitals and by PACS vendors yet. Therefore, even if any modern PACS will accept to store such DICOM STL images, few will render them. There is also a lack of sample files, which strongly calls for an open infrastructure to share knowledge about this standard, to the benefit of hospitals, manufacturers, and researchers.

In this paper, we propose a full software pipeline for the generation, visualization, communication, archiving, and printing of DICOM-compliant 3D models generated from medical images. In our pipeline, the 3D models of anatomical structures can either be automatically derived from DICOM RT-STRUCT instances, that encode the contours of organs at risk in radiotherapy treatment plans, or from binary volumes encoded as NIfTI files, that come from automated tools such as TotalSegmentator. The resulting DICOM 3D models can be displayed using a lightweight Web viewer that is compatible with any Web browser and can be exchanged with other DICOM-compliant systems. Our infrastructure is fully integrated as a plugin to the free and open-source Orthanc ecosystem for medical imaging [15]. Such an open infrastructure can hopefully promote the adoption of DICOM STL by hospitals as an important path to support a consistent, effective deployment of 3D printing across multiple fields of medicine.

2 METHODS

In this section, the main methods used by our software pipeline are presented. Firstly, algorithms suitable for the generation of a 3D models from a 3D bitmap are introduced. Such algorithms are notably applicable to the results of deep learning inference for organ segmentation. Secondly, algorithms for the creation of a 3D bitmap from anatomical structures that have been delineated as part of a regular radiotherapy treatment plan are described. Finally, the encoding of the generated 3D models as DICOM-compliant instances is explained.

2.1 Model generation from volume bitmaps

The central task to the three-dimensional encoding of anatomical structures is to generate a 3D mesh that closely fits a finite, discrete 3D volume, in which each voxel is associated with a binary label (either the voxel belongs to the anatomical structure, in which case it is labeled as "1", or it is not part of the structure, in which case it is labeled as "0"). This output 3D mesh is a list of triangles in the space, each triangle being defined by the coordinates of its three vertices $\vec{x}_i \in \mathbb{R}^3$ where $i \in \{1, 2, 3\}$ and by its unit normal vector $\vec{n} \in \mathbb{R}^3$ pointing outwards from the solid object.

2.1.1 *Marching Cubes.*

The task of surface reconstruction from volume bitmaps is often solved using the *Marching Cubes* algorithm [18, 19]. Marching Cubes is a highly popular algorithm for generating surface representations from regularly sampled volumetric data, with many successful applications [22]. This algorithm consists of a main loop over all the 3D cubic cells whose corners are defined by the voxels of the volume. For each cubic cell, Marching Cubes samples the labels that are associated with its 8 neighboring voxels. Each of the possible combinations of those 8 labels determines one polygon configuration among 256 possible configurations. As an optimization, a pre-computed lookup table for those 256 configurations can be used to speed up the generation of the polygons. The polygon configurations are collected for all the cubic cells and are finally decomposed as 3D triangles to form the output 3D mesh.

An example of application of Marching Cubes to a selected anatomical structure is depicted on Figure 1(a). As can be seen in this example, the drawback of the Marching Cubes algorithm is the staircase shape of the generated 3D meshes. This is a direct consequence of the fact that Marching Cubes is applied locally to the individual cubic cells, without taking larger-scale geometric constraints into account. Therefore, it is most often interesting to post-process the generated 3D mesh by moving the vertices around to minimize some energy function, which makes the global mesh look more natural.

2.1.2 *Laplacian smoothing.*

In this paper, the *Laplacian surface editing* or *Laplacian smoothing* technique is used to soften the staircase shape [13, 30]. Laplacian smoothing is an iterative algorithm that consists in moving each vertex $\vec{x}_i$ of the mesh, by taking into consideration the geometrical relations with its N closest adjacent vertices. For each vertex $\vec{x}_i$ in the 3D mesh, the centroid of its N closest neighbors $\vec{x}_j$ is first computed:

$$\vec{c}_i = \frac{1}{N} \sum_{j=1}^{N} \vec{x}_j. \quad (1)$$

Then, the updated position $\vec{x}'_i$ of the vertex $\vec{x}_i$ is given by slightly pulling the vertex towards the centroid:

$$\vec{x}'_i = \vec{x}_i + \alpha \left(\vec{c}_i - \vec{x}_i \right). \quad (2)$$

The α parameter in Equation 2 is called the *relaxation factor* and is in practice set to 0.1 to avoid large drifts in the positions. This process is repeatedly applied to each vertex of the mesh for a fixed number of iterations (in our case, 15 iterations). Figure 1(b) illustrates the benefits of applying Laplacian smoothing to the meshes generated by the Marching Cubes algorithm. Evidently, Laplacian smoothing

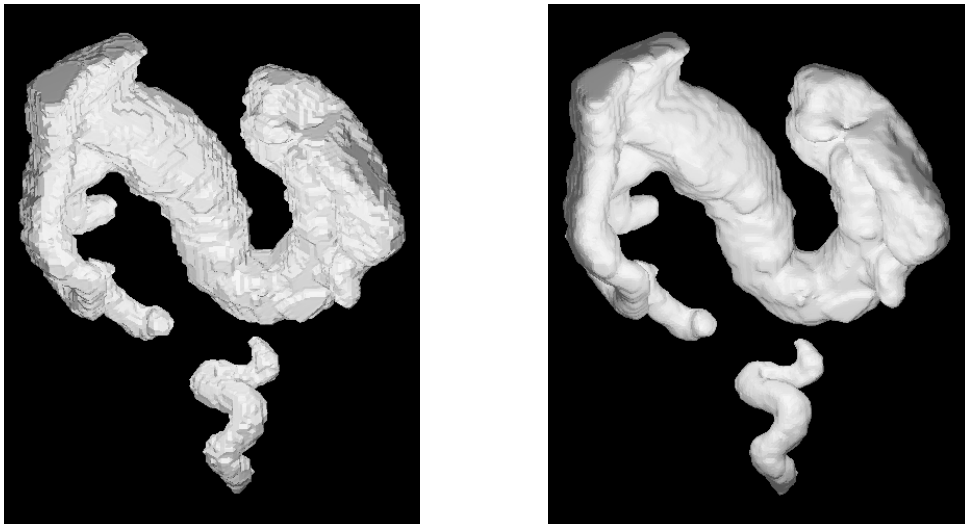

(a) (b)

Figure 1: (a) Generation of a 3D model from a binary volume bitmap corresponding to a human colon[1] using the Marching Cubes algorithm. (b) Laplacian smoothing applied to the same 3D model.

changes the 3D volume that is delimited by the mesh, which might or not be an issue, depending on the application.

In practice, our implementation leverages the well-known free and open-source VTK library [27] to implement both the Marching Cubes and the Laplacian smoothing algorithms.

2.2 Model generation for radiotherapy

The Marching Cubes algorithm described in Section 2.1 takes as input a binary volume bitmap that encodes an anatomical structure of interest. However, such binary bitmaps are most often the outputs of computer vision algorithms and are rarely generated by physicians in the clinical routine. It is thus important to investigate methods that can be applied to present, real-world clinical applications. This has prompted us to turn to radiotherapy. Indeed, radiotherapy is probably the medical specialty that currently manages the largest number of segmented anatomical structures, and for which large datasets are publicly available [10].

2.2.1 Radiotherapy structure sets. In the typical radiotherapy workflow, organs at risk and tumors are delineated by physicians on the axial slices of the simulation CT-scan of the patient, possibly using clues brought by PET-CT-scans and MRI images after proper co-registration with the simulation CT-scan. Such delineated contours are then used to optimize a highly personalized treatment plan for the patient. Given the considerable number of patients receiving radiotherapy treatment worldwide every day, this medical discipline represents a major source of data for the development of algorithms for the segmentation of anatomical structures. In addition, since every patient undergoing radiotherapy has his or her organs at risk delineated, it is possible to generate patient-specific 3D models that could be used for patient education. This motivates the extraction of 3D models corresponding to the anatomical structures of interest using the contours produced in the radiotherapy workflow.

Nonetheless, radiotherapy does not store the delineated contours as volume bitmaps. Instead, any radiotherapy or nuclear medicine software primarily encodes its contours according to the so-called "*Radiation Therapy Structure Set Storage Information Object Definition (IOD)*," often abbreviated as "structure set" or "RT-STRUCT," as specified in the "*PS3.3: Information Object Definitions*" part of the DICOM standard [21]. This standard encoding represents one delineated 3D volume (organ at risk or tumor) as a collection of polygons in the 3D space. Those polygons must comply with several constraints: (a) The vertices of each polygon must be coplanar (i.e., they must lie on the same 3D plane), (b) all the polygons must be parallel, which implies that all the polygons share one common normal vector, and (c) the polygons must be regularly spaced in the 3D space. The encoded 3D volume is defined as the union of the extruded polygons whose thickness is determined by the regular spacing from the latter constraint.

2.2.2 Bitmap generation from a structure set. The conversion of one anatomical structure from a DICOM structure set into a 3D model using the algorithms from Section 2.1 necessitates the anatomical structure to be available as a binary volume bitmap.

To this end, our algorithm begins by determining the normal vector and the thickness of the polygons. This is done by first defining the normal vector $\vec{n} \in \mathbb{R}^3$ that is shared by all the polygons of the structure of interest, as the cross product of the two first segments of the first polygon of the structure set. This normal vector is normalized as a unit vector. Secondly, after verification of coplanarity, all the polygons of the structure are projected onto that unit normal vector, by computing the dot product of one vertex in the polygon with the unit normal vector. This operation generates an array of real numbers, one for each polygon, that represents the

[1] This sample bitmap corresponds to the `colon.nii.gz` reference file that is part of the source distribution of TotalSegmentator [35].

offsets of the polygons in the space, and that is expected to follow a 1D periodic pattern because of the constraint on the regular spacing between the polygons. This array is sorted and duplicated values are removed from it. Thirdly, another array is generated as the difference between two successive numbers in the sorted array. This new array is also sorted. At this point, the first element of this new array defines the thickness of the polygons. If the structure set is well-conditioned, the other elements of the new array should be integer multiples of the computed thickness.

Once the normal vector and the thickness of the polygons have been extracted, the geometry of the volume bitmap can be determined. The physical extent of the volume along the z−axis is given by the difference between the maximum and minimum values of the projection onto the unit normal vector. The discrete depth of the bitmap is taken as the division of the latter physical extent by the thickness, which corresponds to an integer value by construction. On the other hand, the physical extent of the volume along the x−axis and the y−axis is determined by the minimum and maximum values of the projection (i.e., the dot product) of each vertex of each polygon over the direction cosines that are available in the "*Image Orientation Patient*" `(0x0020, 0x0037)` DICOM tag of the referenced CT image. The discrete width and height of the volume bitmap are assumed to be specified by the user.

Next, the content of the volume bitmap is generated by a loop over the polygons of interest. Each of those polygons corresponds to one single slice in the volume bitmap, which is determined by the projection of one of its vertices along the unit normal vector. The 3D coordinates of the vertices are then projected onto the 2D plane defined by the "*Image Orientation Patient*" DICOM tag, which gives the coordinates of a 2D polygon. The resulting 2D polygon can then be drawn onto the target slice of the volume bitmap by a regular scan-line polygon filling algorithm. Note that an XOR operation is used during the filling, as some DICOM RT-STRUCT instances encode holes in a structure set as overlapping polygons.

Finally, to have a common aspect ratio along the x−axis, the y−axis, and the z−axis, the depth of the volume bitmap is resized with interpolation to match the width and height provided by the user. The Marching Cubes algorithm is then readily applicable. Figure 2 shows the result of the generation of a 3D mesh from a DICOM structure set, including Laplacian smoothing.

2.3 Encapsulation of STL into DICOM

The previous sections have explained how to create 3D meshes, either from volume bitmaps, or from radiotherapy structure sets. As explained in Section 2.1.1, a 3D mesh is a collection of triangle facets. It is then straightforward to create a binary STL file that encodes the 3D mesh, as such a file is simply made of a header followed by the list of triangles associated with their normal vector.

As explained in the introduction, Supplement 205 of DICOM introduced the so-called "*Encapsulated STL Information Object Description (IOD)*" to encapsulate an arbitrary STL file into a DICOM envelope. The encapsulation process consists in first identifying the DICOM study that will act as the parent of the 3D mesh, then copying the content of the patient-level and study-level modules of this parent study to form the skeleton of the new DICOM instance. The encapsulation process then basically boils down

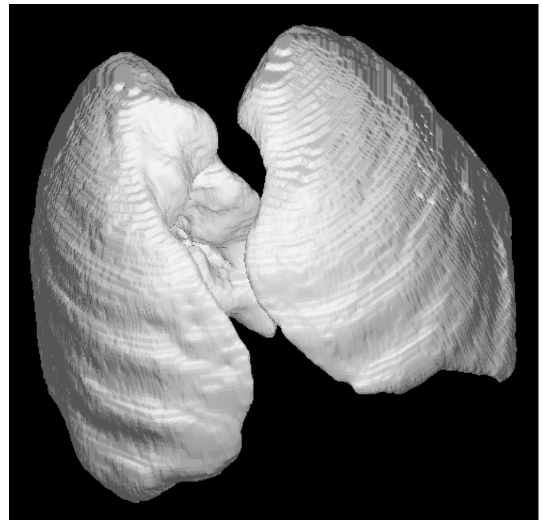

Figure 2: 3D model of the lungs extracted from a DICOM RT-STRUCT instance from the *Lung CT Segmentation Challenge 2017* (LCTSC) dataset [36, 37] provided by *The Cancer Imaging Archive* project [10].

to setting additional DICOM tags in this new DICOM instance, the most important being: "*SOP Class UID*" `(0x0008, 0x0016)` that must be set to "`1.2.840.10008.5.1.4.1.1.104.3`", "*Modality*" `(0x0008, 0x0060)` to "`M3D`", "*MIME Type Of Encapsulated Document*" `(0x0042, 0x0012)` to "`model/stl`", and "*Encapsulated Document*" `(0x0042, 0x0011)` must contain the raw STL file[2]. Once the DICOM instance is created, it can be stored by any PACS server (which notably enables the long-term archiving of the 3D model, as well as the smooth integration with the Electronic Health Records of the hospital), then exchanged thanks to the DICOM and DICOMweb protocols.

3 APPLICATION

Section 2 has introduced methods that can be used to generate, then encode 3D meshes that represent anatomical structures in an interoperable way thanks to the DICOM standard. In this section, we propose a concrete implementation of those methods that can be deployed in companies, in research institutions, and in hospitals.

Orthanc is a well-known free and open-source ecosystem for medical imaging [15]. It provides a reference implementation of a PACS server. Orthanc also embeds a Web server that is primarily used to provide a REST API to manipulate the content of the server. Moreover, Orthanc features support for plugins, which can be used to extend its built-in REST API by adding new routes, as well as to enrich its default Web user interface.

In this paper, we extend Orthanc with a new plugin that adds support for Encapsulated STL Information Object Description. Figure 3 depicts the first feature of this plugin. Whenever the plugin detects that the Web interface of Orthanc is showing a DICOM instance that encapsulates a STL file, it displays a button that opens

[2] Note that the `dciodvfy` command-line tool from the `dicom3tools` software can be used to check the validity of the created DICOM instances.

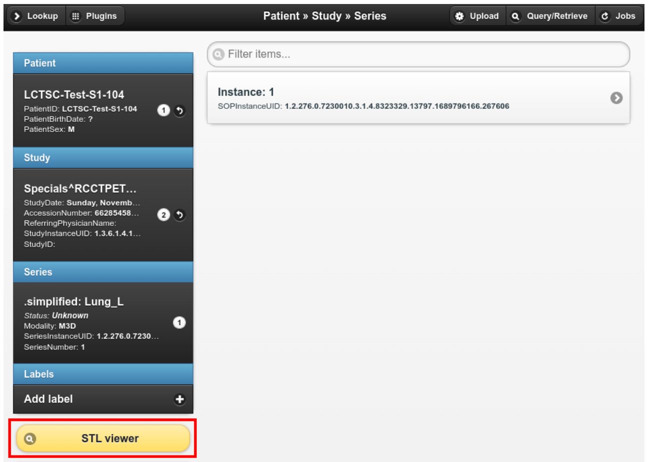

Figure 3: Web user interface to open a lightweight Web viewer of DICOM STL models. Figures 1 and 2 correspond to actual screenshots of this viewer.

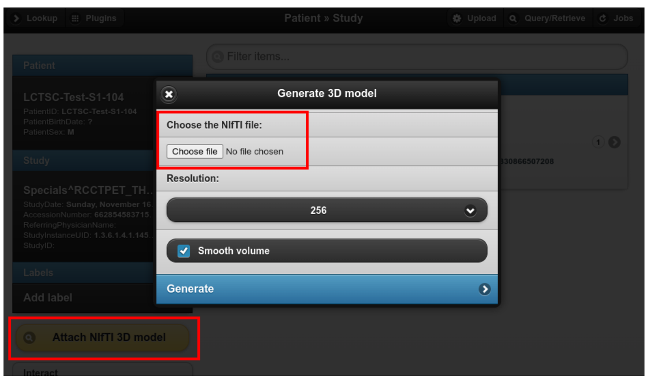

Figure 4: User interface to generate a DICOM STL instance from a volume bitmap, and to attach the generated instance to an existing DICOM study.

a basic lightweight Web viewer to render this STL file. This Web viewer is compatible with any modern Web browser and is built using the Three.js JavaScript library[3]. This feature provides an intuitive, immediate user interface to handle DICOM STL instances, including those coming from other sources than Orthanc.

As a second feature, the STL plugin for Orthanc can be used to attach a 3D mesh generated from a binary volume bitmap to an existing DICOM study, following the algorithms of Section 2.1.1. This feature is depicted in Figure 4. The input volume bitmap must be encoded according to the NIfTI file format, although support for other input formats could easily be added. The user interface allows to resize the volume bitmap to a given resolution, as well as to choose whether Laplacian smoothing is applied or not. The plugin then generates a new DICOM STL instance that is stored inside Orthanc as a part of the selected DICOM study. Thanks to this feature, it is notably immediate to archive, then share with other users a 3D mesh generated from a segmentation bitmap produced by TotalSegmentator [35], which is a recent software for the automated segmentation of up to 104 different anatomical structures that leverages the nnU-Net deep learning framework [14].

[3]Internally, the viewer calls the route `/instances/{id}/stl` that is added to the REST API of Orthanc by the plugin, in order to unwrap the STL file out of some DICOM instance of interest whose Orthanc identifier is given by `id`. Note that this route can also be used by external applications to retrieve the raw STL file encapsulated inside a DICOM instance.

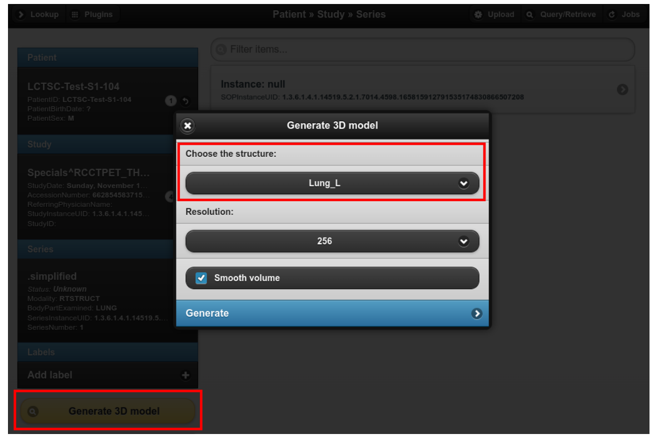

Figure 5: User interface to generate a 3D model from one structure of interest in a DICOM RT-STRUCT instance.

Thirdly, as illustrated in Figure 5, the STL plugin for Orthanc can be used to generate a 3D model out of a DICOM structure set, following the algorithms of Section 2.2. This feature is available once the user interface of Orthanc is displaying a DICOM RT-STRUCT series. As can be seen in the screenshot, the user can select the structure of interest, the resolution of the intermediate volume bitmap, and whether Laplacian smoothing should be applied.

These two possibilities for generating 3D models are also programmatically accessible as two new routes in the REST API of Orthanc that are added by the plugin: The route `/stl/encode-nifti` can be used to generate DICOM STL instances from NIfTI files, whereas the route `/stl/encode-rtstruct` will generate DICOM STL instances from DICOM RT-STRUCT instances. External applications dealing with radiotherapy, nuclear medicine, or organ segmentation can thus use Orthanc to easily generate, store and archive their 3D models in an interoperable way.

Finally, besides the topic of interoperability, this work was also motivated by providing a pathway to ease the 3D printing of anatomical structures that could be accessible to physicians. We have thus validated whether the 3D meshes that are produced by the STL plugin for Orthanc from a DICOM structure set can be printed by a regular 3D printer. The results are shown in Figure 6, which proves that our software pipeline is effective, from the generation of DICOM-compliant 3D meshes, to the printing of 3D models. The source code of the STL plugin for Orthanc is fully available as free and open-source software released under the GPLv3 license, at address: https://orthanc.uclouvain.be/hg/orthanc-stl/.

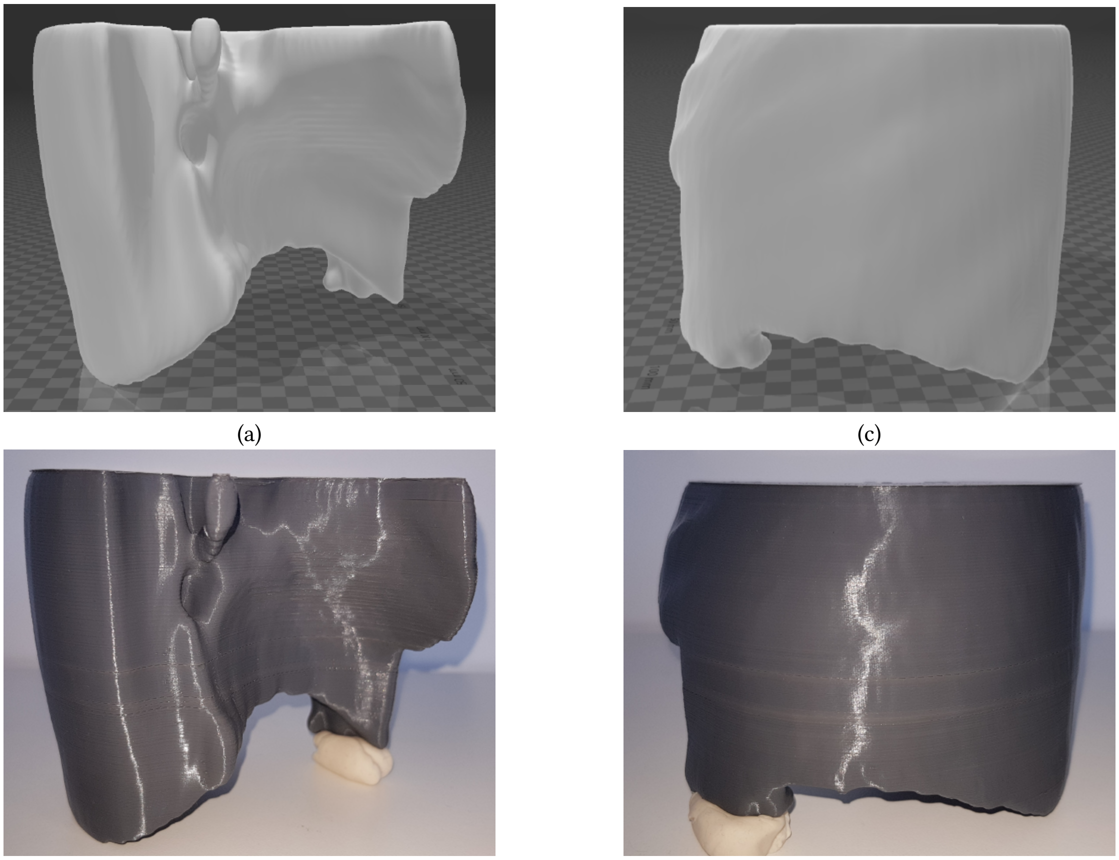

(a) (c) (b) (d)

Figure 6: Comparison of a 3D model of an anatomical structure generated by the STL plugin for Orthanc, against its 3D printed version created by an Ultimaker 3 printer. (a) and (b) correspond to the back part of the left lung, while (c) and (d) correspond to the front part of the left lung.

4 CONCLUSION

In this paper, we have proposed a software pipeline that can be used to generate 3D models from volume bitmaps or from DICOM structure sets, then to encode those models according to the DICOM interoperability standard. This DICOM-based workflow allows to close the gap between 3D printing and medical imaging, by storing the models directly inside the PACS, and by enabling effective indexing, archiving, and sharing of the 3D models. Our software takes the form of a free and open-source plugin for Orthanc, which provides an accessible, easy-to-use Web interface to display and generate DICOM STL models in one click. Altogether, this contribution could open the path to new applications in medical disciplines leveraging 3D printing, as well as in patient education.

Future work will consist in interfacing existing free and open-source slicer software for 3D printing, such as Ultimaker Cura or derivatives of Slic3r, with the REST API of Orthanc, so that Orthanc can seamlessly be used as a source of STL models in the slicer software. Another important work will be to integrate deep learning models for organ segmentation directly inside the STL plugin for Orthanc. Such an integration would avoid the need to use external software such as TotalSegmentator, hereby facilitating the software deployment and improving the overall user experience.

REFERENCES

[1] Sharon A. Abbott. 1998. The Benefits of Patient Education. *Gastroenterology Nursing* 21, 5 (Oct. 1998), 207.

[2] L. E. I. A'Campo, E. M. Wekking, N. G. A. Spliethoff-Kamminga, S. Le Cessie, and R. A. C. Roos. 2010. The benefits of a standardized patient education program for patients with Parkinson's disease and their caregivers. *Parkinsonism & Related Disorders* 16, 2 (Feb. 2010), 89–95. https://doi.org/10.1016/j.parkreldis.2009.07.009

[3] Ciro Andolfi, Alejandro Plana, Patrick Kania, P. Pat Banerjee, and Stephen Small. 2017. Usefulness of Three-Dimensional Modeling in Surgical Planning, Resident Training, and Patient Education. *Journal of Laparoendoscopic & Advanced Surgical Techniques* 27, 5 (May 2017), 512–515. https://doi.org/10.1089/lap.2016.0421 Publisher: Mary Ann Liebert, Inc., publishers.

[4] Manjusha Annaji, Sindhu Ramesh, Ishwor Poudel, Manoj Govindarajulu, Robert D. Arnold, Muralikrishnan Dhanasekaran, and R. Jayachandra Babu. 2020. Application of Extrusion-Based 3D Printed Dosage Forms in the Treatment of Chronic Diseases. *Journal of Pharmaceutical Sciences* 109, 12 (Dec. 2020), 3551–3568. https://doi.org/10.1016/j.xphs.2020.09.042

[5] Edward E. Bartlett. 1995. Cost-benefit analysis of patient education. *Patient Education and Counseling* 26, 1 (Sept. 1995), 87–91. https://doi.org/10.1016/0738-3991(95)00723-D

[6] Jean-Christophe Bernhard, Shuji Isotani, Toru Matsugasumi, Vinay Duddalwar, Andrew J. Hung, Evren Suer, Eduard Baco, Raj Satkunasivam, Hooman Djaladat, Charles Metcalfe, Brian Hu, Kelvin Wong, Daniel Park, Mike Nguyen, Darryl Hwang, Soroush T. Bazargani, Andre Luis de Castro Abreu, Monish Aron, Osamu

Ukimura, and Inderbir S. Gill. 2016. Personalized 3D printed model of kidney and tumor anatomy: a useful tool for patient education. *World Journal of Urology* 34, 3 (March 2016), 337–345. https://doi.org/10.1007/s00345-015-1632-2

[7] Hong Cai, Zhongjun Liu, Feng Wei, Miao Yu, Nanfang Xu, and Zihe Li. 2018. 3D Printing in Spine Surgery. *Advances in Experimental Medicine and Biology* 1093 (2018), 345–359. https://doi.org/10.1007/978-981-13-1396-7_27

[8] James Castiglione, Elanchezhian Somasundaram, Leah A. Gilligan, Andrew T. Trout, and Samuel Brady. 2021. Automated Segmentation of Abdominal Skeletal Muscle on Pediatric CT Scans Using Deep Learning. *Radiology: Artificial Intelligence* 3, 2 (March 2021), e200130. https://doi.org/10.1148/ryai.2021200130 Publisher: Radiological Society of North America.

[9] Eva Marie Castro, Tine Van Regenmortel, Kris Vanhaecht, Walter Sermeus, and Ann Van Hecke. 2016. Patient empowerment, patient participation and patient-centeredness in hospital care: A concept analysis based on a literature review. *Patient Education and Counseling* 99, 12 (Dec. 2016), 1923–1939. https://doi.org/10.1016/j.pec.2016.07.026

[10] Kenneth Clark, Bruce Vendt, Kirk Smith, John Freymann, Justin Kirby, Paul Koppel, Stephen Moore, Stanley Phillips, David Maffitt, Michael Pringle, Lawrence Tarbox, and Fred Prior. 2013. The Cancer Imaging Archive (TCIA): Maintaining and Operating a Public Information Repository. *Journal of Digital Imaging* 26, 6 (July 2013), 1045–1057. https://doi.org/10.1007/s10278-013-9622-7

[11] Daniel F. Craft, Stephen F. Kry, Peter Balter, Mohammad Salehpour, Wendy Woodward, and Rebecca M. Howell. 2018. Material matters: Analysis of density uncertainty in 3D printing and its consequences for radiation oncology. *Medical Physics* 45, 4 (March 2018), 1614–1621. https://doi.org/10.1002/mp.12839

[12] Anurup Ganguli, Gelson J. Pagan-Diaz, Lauren Grant, Caroline Cvetkovic, Mathew Bramlet, John Vozenilek, Thenkurussi Kesavadas, and Rashid Bashir. 2018. 3D printing for preoperative planning and surgical training: a review. *Biomedical Microdevices* 20, 3 (Aug. 2018), 65. https://doi.org/10.1007/s10544-018-0301-9

[13] Leonard R. Herrmann. 1976. Laplacian-Isoparametric Grid Generation Scheme. *Journal of the Engineering Mechanics Division* 102, 5 (Oct. 1976), 749–756. https://doi.org/10.1061/JMCEA3.0002158 Publisher: American Society of Civil Engineers.

[14] Fabian Isensee, Jens Petersen, Andre Klein, David Zimmerer, Paul F. Jaeger, Simon Kohl, Jakob Wasserthal, Gregor Koehler, Tobias Norajitra, Sebastian Wirkert, and Klaus H. Maier-Hein. 2018. nnU-Net: Self-adapting Framework for U-Net-Based Medical Image Segmentation. https://doi.org/10.48550/ARXIV.1809.10486

[15] Sébastien Jodogne. 2018. The Orthanc Ecosystem for Medical Imaging. *Journal of Digital Imaging* 31, 3 (May 2018), 341–352. https://doi.org/10.1007/s10278-018-0082-y

[16] Nancy Kruzik. 2009. Benefits of Preoperative Education for Adult Elective Surgery Patients. *AORN Journal* 90, 3 (Sept. 2009), 381–387. https://doi.org/10.1016/j.aorn.2009.06.022

[17] Hsiu-Hsia Lin, Daniel Lonic, and Lun-Jou Lo. 2018. 3D printing in orthognathic surgery, A literature review. *Journal of the Formosan Medical Association* 117, 7 (July 2018), 547–558. https://doi.org/10.1016/j.jfma.2018.01.008

[18] William E. Lorensen and Harvey E. Cline. 1987. Marching cubes: A high resolution 3D surface construction algorithm. *ACM SIGGRAPH Computer Graphics* 21, 4 (Aug. 1987), 163–169. https://doi.org/10.1145/37402.37422

[19] William E. Lorensen and Harvey E. Cline. 1998. Marching cubes: a high resolution 3D surface construction algorithm. In *Seminal graphics*. ACM, New York, NY, USA, 347–353. https://doi.org/10.1145/280811.281026

[20] Jonathan M. Morris, Adam Wentworth, Matthew T. Houdek, S. Mohammed Karim, Michelle J. Clarke, David J. Daniels, and Peter S. Rose. 2023. The Role of 3D Printing in Treatment Planning of Spine and Sacral Tumors. *Neuroimaging Clinics of North America* 33, 3 (Aug. 2023), 507–529. https://doi.org/10.1016/j.nic.2023.05.001

[21] National Electrical Manufacturers Association. 2023. ISO 12052 / NEMA PS3, Digital Imaging and Communications in Medicine (DICOM) Standard. http://www.dicomstandard.org

[22] G.M. Nielson. 2003. On marching cubes. *IEEE Transactions on Visualization and Computer Graphics* 9, 3 (July 2003), 283–297. https://doi.org/10.1109/TVCG.2003.1207437 Conference Name: IEEE Transactions on Visualization and Computer Graphics.

[23] Luigi Pugliese, Stefania Marconi, Erika Negrello, Valeria Mauri, Andrea Peri, Virginia Gallo, Ferdinando Auricchio, and Andrea Pietrabissa. 2018. The clinical use of 3D printing in surgery. *Updates in Surgery* 70, 3 (Sept. 2018), 381–388. https://doi.org/10.1007/s13304-018-0586-5

[24] Raffaele Pugliese, Benedetta Beltrami, Stefano Regondi, and Christian Lunetta. 2021. Polymeric biomaterials for 3D printing in medicine: An overview. *Annals of 3D Printed Medicine* 2 (June 2021), 100011. https://doi.org/10.1016/j.stlm.2021.100011

[25] Michael K. Rooney, David M. Rosenberg, Steve Braunstein, Adam Cunha, Antonio L. Damato, Eric Ehler, Todd Pawlicki, James Robar, Ken Tatebe, and Daniel W. Golden. 2020. Three-dimensional printing in radiation oncology: A systematic review of the literature. *Journal of Applied Clinical Medical Physics* 21, 8 (May 2020), 15–26. https://doi.org/10.1002/acm2.12907

[26] Ian M. Sander, Taimi T. Liepert, Evan L. Doney, W. Matthew Leevy, and Douglas R. Liepert. 2017. Patient Education for Endoscopic Sinus Surgery: Preliminary Experience Using 3D-Printed Clinical Imaging Data. *Journal of Functional Biomaterials* 8, 2 (June 2017), 13. https://doi.org/10.3390/jfb8020013 Number: 2 Publisher: Multidisciplinary Digital Publishing Institute.

[27] Will Schroeder, Ken Martin, and Bill Lorensen. 2006. *The Visualization Toolkit (4th ed.)*. Kitware, New York.

[28] Pratik Shah and B. S. Chong. 2018. 3D imaging, 3D printing and 3D virtual planning in endodontics. *Clinical Oral Investigations* 22, 2 (March 2018), 641–654. https://doi.org/10.1007/s00784-018-2338-9

[29] Neeraj Sharma and Lalit M. Aggarwal. 2010. Automated medical image segmentation techniques. *Journal of Medical Physics / Association of Medical Physicists of India* 35, 1 (2010), 3–14. https://doi.org/10.4103/0971-6203.58777

[30] O. Sorkine, D. Cohen-Or, Y. Lipman, M. Alexa, C. Rössl, and H.-P. Seidel. 2004. Laplacian surface editing. In *Proceedings of the 2004 Eurographics/ACM SIGGRAPH symposium on Geometry processing (SGP '04)*. Association for Computing Machinery, New York, NY, USA, 175–184. https://doi.org/10.1145/1057432.1057456

[31] Israel Valverde. 2017. Three-dimensional Printed Cardiac Models: Applications in the Field of Medical Education, Cardiovascular Surgery, and Structural Heart Interventions. *Revista Española de Cardiología (English Edition)* 70, 4 (April 2017), 282–291. https://doi.org/10.1016/j.rec.2017.01.012

[32] Marijke van der Linde-van den Bor, Fiona Slond, Omayra C. D. Liesdek, Willem J. Suyker, and Saskia W. M. Weldam. 2022. The use of virtual reality in patient education related to medical somatic treatment: A scoping review. *Patient Education and Counseling* 105, 7 (July 2022), 1828–1841. https://doi.org/10.1016/j.pec.2021.12.015

[33] Nicole Wake, Andrew B. Rosenkrantz, Richard Huang, Katalina U. Park, James S. Wysock, Samir S. Taneja, William C. Huang, Daniel K. Sodickson, and Hersh Chandarana. 2019. Patient-specific 3D printed and augmented reality kidney and prostate cancer models: impact on patient education. *3D Printing in Medicine* 5, 1 (Feb. 2019), 4. https://doi.org/10.1186/s41205-019-0041-3

[34] David Walker, Ade Adebajo, and Marwan Bukhari. 2020. The benefits and challenges of providing patient education digitally. *Rheumatology* 59, 12 (Dec. 2020), 3591–3592. https://doi.org/10.1093/rheumatology/keaa642

[35] Jakob Wasserthal, Hanns-Christian Breit, Manfred T. Meyer, Maurice Pradella, Daniel Hinck, Alexander W. Sauter, Tobias Heye, Daniel Boll, Joshy Cyriac, Shan Yang, Michael Bach, and Martin Segeroth. 2023. TotalSegmentator: Robust Segmentation of 104 Anatomic Structures in CT Images. *Radiology: Artificial Intelligence* (July 2023). https://doi.org/10.1148/ryai.230024

[36] Jinzhong Yang, Greg Sharp, Harini Veeraraghavan, Wouter Van Elmpt, Andre Dekker, Tim Lustberg, and Mark Gooding. 2017. Data from Lung CT Segmentation Challenge. https://doi.org/10.7937/K9/TCIA.2017.3R3FVZ08

[37] Jinzhong Yang, Harini Veeraraghavan, Samuel G. Armato, Keyvan Farahani, Justin S. Kirby, Jayashree Kalpathy-Kramer, Wouter van Elmpt, Andre Dekker, Xiao Han, Xue Feng, Paul Aljabar, Bruno Oliveira, Brent van der Heyden, Leonid Zamdborg, Dao Lam, Mark Gooding, and Gregory C. Sharp. 2018. Autosegmentation for thoracic radiation treatment planning: A grand challenge at AAPM 2017. *Medical Physics* 45, 10 (Sept. 2018), 4568–4581. https://doi.org/10.1002/mp.13141

[38] Tianyou Yang, Tianbao Tan, Jiliang Yang, Jing Pan, Chao Hu, Jiahao Li, and Yan Zou. 2018. The impact of using three-dimensional printed liver models for patient education. *Journal of International Medical Research* 46, 4 (April 2018), 1570–1578. https://doi.org/10.1177/0300060518755267 Publisher: SAGE Publications Ltd.

[39] Yuan-dong Zhuang, Mao-chao Zhou, Shi-chao Liu, Jian-feng Wu, Rui Wang, and Chun-mei Chen. 2019. Effectiveness of personalized 3D printed models for patient education in degenerative lumbar disease. *Patient Education and Counseling* 102, 10 (Oct. 2019), 1875–1881. https://doi.org/10.1016/j.pec.2019.05.006

[40] Matthew J. Zirwas and Jessica L. Holder. 2009. Patient Education Strategies in Dermatology. *The Journal of Clinical and Aesthetic Dermatology* 2, 12 (Dec. 2009), 24–27. https://www.ncbi.nlm.nih.gov/pmc/articles/PMC2923943/